Am J Physiol Cell Physiol 293: C1924–C1933, 2007.
First published October 10, 2007; doi:10.1152/ajpcell.00555.2006.

Regulation of cAMP dynamics by Ca^{2+} and G protein-coupled receptors in the pancreatic β-cell: a computational approach

Leonid E. Fridlyand, Mark C. Harbeck, Michael W. Roe, and Louis H. Philipson

Department of Medicine, University of Chicago, Chicago, Illinois

Submitted 31 October 2006; accepted in final form 1 October 2007

Fridlyand LE, Harbeck MC, Roe MW, Philipson LH. Regulation of cAMP dynamics by Ca^{2+} and G protein-coupled receptors in the pancreatic β-cell: a computational approach. *Am J Physiol Cell Physiol* 293: C1924–C1933, 2007. First published October 10, 2007; doi:10.1152/ajpcell.00555.2006.—In this report we describe a mathematical model for the regulation of cAMP dynamics in pancreatic β-cells. Incretin hormones such as glucagon-like peptide 1 (GLP-1) increase cAMP and augment insulin secretion in pancreatic β-cells. Imaging experiments performed in MIN6 insulinoma cells expressing a genetically encoded cAMP biosensor and loaded with fura-2, a calcium indicator, showed that cAMP oscillations are differentially regulated by periodic changes in membrane potential and GLP-1. We modeled the interplay of intracellular calcium (Ca^{2+}) and its interaction with calmodulin, G protein-coupled receptor activation, adenylyl cyclases (AC), and phosphodiesterases (PDE). Simulations with the model demonstrate that cAMP oscillations are coupled to cytoplasmic Ca^{2+} oscillations in the β-cell. Slow Ca^{2+} oscillations (<1 min^{-1}) produce low-frequency cAMP oscillations, and faster Ca^{2+} oscillations (>3–4 min^{-1}) entrain high-frequency, low-amplitude cAMP oscillations. The model predicts that GLP-1 receptor agonists induce cAMP oscillations in phase with cytoplasmic Ca^{2+} oscillations. In contrast, observed antiphasic Ca^{2+} and cAMP oscillations can be simulated following combined glucose and tetraethylammonium-induced changes in membrane potential. The model provides additional evidence for a pivotal role for Ca^{2+}-dependent AC and PDE activation in coupling of Ca^{2+} and cAMP signals. Our results reveal important differences in the effects of glucose/TEA and GLP-1 on cAMP dynamics in MIN6 β-cells.

adenylyl cyclase; calcium ion; glucagon-like peptide 1; modeling; oscillations

PANCREATIC β-CELLS SECRETE insulin following an increase in blood glucose concentration. Under physiological conditions, secretion of insulin is tightly regulated and depends on increases, often oscillatory, in cytoplasmic Ca^{2+} concentration ($[Ca^{2+}]_i$). Glucose-induced insulin secretion is regulated by signals produced by glucose metabolism that initially affect plasma membrane potential and $[Ca^{2+}]_i$. Adenosine 3′,5′-cyclic monophosphate (cAMP) signaling pathways are also important in regulating β-cell secretion (6, 17, 22). The cAMP signaling pathway involves both secretory regulatory cascades and gene expression.

The hallmark of secretion-stimulating hormones known as incretins, in particular glucagon-like peptide 1 (GLP-1) and glucose-dependent insulinotropic polypeptide (GIP), is the activation of cAMP cascades in the β-cell following activation of adenylyl cyclases (AC) (13, 21, 37). Inhibition of cAMP cascades can also occur via receptors coupled to inhibitory G proteins. For example, the α-adrenergic agonists somatostatin and galanin decrease cAMP levels in part by inhibiting AC (37) (Fig. 1). cAMP activates protein kinase A, a multifunctional regulatory enzyme (37), while other pathways involve initial binding to the guanyl exchange proteins EPAC1 and EPAC2 (exchange proteins activated by cAMP) (22).

In pancreatic β-cells, increased cAMP leads to increased activity of voltage-dependent calcium channels (VDCC) (26, 37), decreased ATP-sensitive potassium (K_{ATP}) channel conductance (17, 24), and increased activity of inositol 1,4,5-trisphosphate (IP_3) receptors in the endoplasmic reticulum contributing to calcium-induced Ca^{2+} release (7, 23, 25, 35), among other effects. Changes in Ca^{2+} influx when cAMP levels are elevated can also modulate cAMP dynamics. These findings and other recent studies suggest that Ca^{2+} and cAMP are dynamically regulated to form a network that produces diverse temporal signaling patterns in β-cells (8, 28). The temporal and causal interplay between Ca^{2+} and cAMP may reflect a higher order organization of second messenger signaling cascades that determine specificity of cellular responses to extracellular stimuli (28).

We sought to better understand the temporal and causal relationships between Ca^{2+} and cAMP by incorporating cAMP dynamics into our developing computational model of β-cell signal transduction. This model incorporates interactions among $[Ca^{2+}]_i$, Ca^{2+}-bound calmodulin (Ca^{2+}/CaM), and recent data on cAMP dynamics. The results with this new model indicate that specific isoforms of AC and phosphodiesterase (PDE) could effectively influence and synchronize cAMP dynamics. In addition, changes in cytoplasmic cAMP concentration ($[cAMP]_i$) can feed back on Ca^{2+} dynamics in the β-cell. This dramatically different view of cAMP regulation in the β-cell could have important implications for understanding incretin effects as well as new pharmacological approaches to the treatment of diabetes that directly or indirectly modulate β-cell cAMP levels.

METHODS

Experimental Procedures

cAMP and Ca^{2+} imaging. Simultaneous measurements of $[cAMP]_i$ and $[Ca^{2+}]_i$ were performed as previously described (28). Briefly, MIN6 cells transiently transfected with Epac1-camps, a unimolecular fluorescence resonance energy transfer (FRET)-based indicator of cAMP (32), were loaded with 1 μM fura-2 acetoxymethyl ester (Molecular Probes) for 15–20 min at 37°C in Krebs-Ringer bicarbonate solution containing 119 mM NaCl, 4.7 mM KCl, 2.5 mM $CaCl_2$, 1 mM $MgCl_2$, 1 mM KH_2PO_4, 25 mM $NaHCO_3$, 10 mM HEPES-NaOH (pH 7.40), and 12 mM glucose. Cells were imaged using an inverted fluorescence microscope (Nikon TE-2000U) equipped with a 16-bit Cascade 650 digital camera (Roper Instruments). Excitation wavelength for Epac1-camps was 440 nm. Dual-wavelength emission ratio imaging at 485 nm (FRET donor, enhanced cyan fluorescent protein) and 535 nm (FRET acceptor, enhanced yellow fluorescent

Address for reprint requests and other correspondence: L. E. Fridlyand, Dept. of Medicine, MC-1027, The Univ. of Chicago, 5841 S. Maryland Ave., Chicago, IL 60637 (e-mail: lfridlia@medicine.bsd.uchicago.edu).

The costs of publication of this article were defrayed in part by the payment of page charges. The article must therefore be hereby marked "*advertisement*" in accordance with 18 U.S.C. Section 1734 solely to indicate this fact.

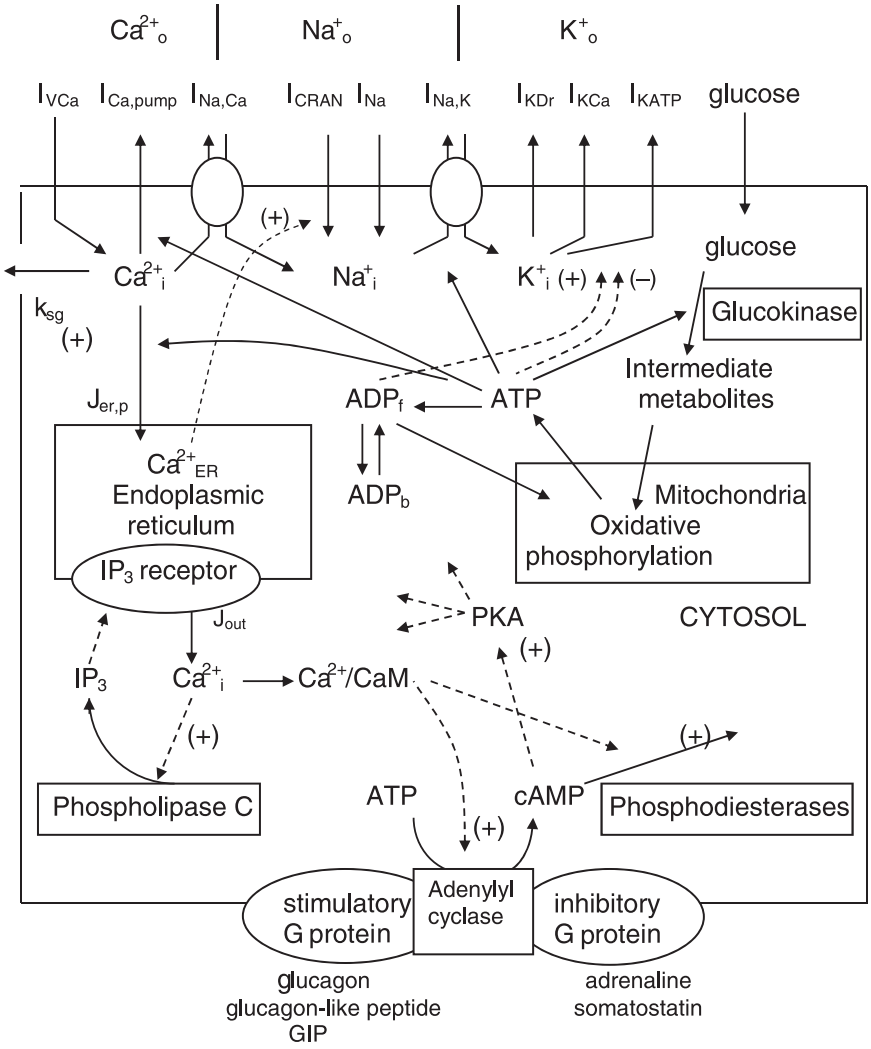

Fig. 1. Interaction among ions, membrane channel conductances, and the mechanism of cAMP regulation included in the β-cell model. Plasma membrane currents (*top*) include voltage-dependent Ca^{2+} current (I_{VCa}), a Ca^{2+} pump current ($I_{Ca,pump}$), Na^+/Ca^{2+} exchange current ($I_{Na,Ca}$), Ca^{2+} release-activated nonselective cation current (I_{CRAN}), inward Na^+ current (I_{Na}), a Na^+-K^+ pump current ($I_{Na,K}$), a delayed rectifying K^+ current (I_{KDr}), the voltage-independent small-conductance Ca^{2+}-activated K^+ current (I_{KCa}), and ATP-sensitive K^+ current (I_{KATP}). k_{sg} is a coefficient of the sequestration rate of Ca^{2+} by the secretory granules, $J_{er,p}$ is an uptake of Ca^{2+} by endoplasmic reticulum (ER), and J_{out} is Ca^{2+} leak current from ER. IP_3, inositol 1,4,5-trisphosphate. ATP is the free cytosolic form of ATP, ADP_f is free cytosolic ADP, and MgADP and ADP_b are bound cytosolic ADP and MgADP; Ca^{2+}/CaM is Ca^{2+}-bound calmodulin. Synthesis and degradation of cAMP were catalyzed by adenylyl cyclase (AC) and phosphodiesterase (PDE), respectively. AC was activated by stimulatory G protein and Ca^{2+}/CaM and deactivated by inhibited G protein, whereas PDE activity was enhanced by Ca^{2+}/CaM. Solid lines indicate flux of metabolic substrates, and dashed lines indicate inhibitory or stimulatory influences on currents or fluxes.

protein) was accomplished using a computer-controlled high-speed filter wheel (Lambda 10-2 optical filter changer; Sutter Instrument, Novato, CA). Images were captured at 10-s intervals; 340- and 380-nm excitation filters and a 520-nm emission filter were used for fura-2 dual-wavelength excitation ratio imaging. A 455-nm dichroic filter (Chroma Technology, Brattelboro, VT) was used for Epac1-camps and fura-2. Image acquisition and data analysis were accomplished using MetaMorph/MetaFluor software (Universal Imaging). Data are expressed as the ratio of FRET donor and acceptor emission ($R_{485/535}$) and the fura-2 340- and 380-nm excitation ($R_{340/380}$) and normalized to the average baseline values of $R_{485/535}$ and $R_{340/380}$ as described previously (20, 25).

Modeling Procedures

We modeled $[Ca^{2+}]_i$ and $[cAMP]_i$ dynamics by employing defined parameters regulating Ca^{2+} transport and redistribution processes as well as cAMP production and degradation in a single β-cell. The reaction network of the model consists of two parts: *1*) channels, pumps, and exchangers that describe plasma membrane ion fluxes and *2*) a fluid compartment model that describes processes associated with the regulation of Ca^{2+}, Na^+, ATP, ADP, IP_3, Ca^{2+}/CaM, and cAMP in cytoplasm and Ca^{2+} in the endoplasmic reticulum (ER) (Fig. 1). The model accounts for Ca^{2+} transport processes known to be present in β-cells: Ca^{2+} release from and uptake into the ER, and Ca^{2+} extrusion and entry across the plasma membrane. The main features of the model other than those reflecting cAMP regulation have been described previously (11, 12). This model does not take into account possible subcellular compartmentalization of cAMP, AC, or PDE, which is an important regulatory mechanism in larger cell types such as cardiomyocytes (4) or in human astrocytoma cells (15). The importance of cAMP compartmentalization in pancreatic β-cells is unclear.

This model does not attempt to include all the possible factors involved in the effects of cAMP, but to illustrate the utility of our model, we have simulated the effects of the cAMP pathway on specific ion channels. This model is available for direct simulation on the website "Virtual Cell" (www.nrcam.uchc.edu) in the "MathModel Database" on the "math workspace" in the library "Fridlyand" with the name "cAMP".

Multiple isoforms of AC and PDE are regulated by Ca^{2+} and Ca^{2+}-bound calmodulin, defined as Ca^{2+}/CaM (4, 15). For this reason, our description of the regulation of Ca^{2+} dynamics was extended to include their interactions. Ca^{2+} binds to calmodulin (CaM) in four steps and generates four species of Ca^{2+}-bound CaM with one (Ca_1CaM), two (Ca_2CaM), three (Ca_3CaM) and four (Ca_4CaM) Ca^{2+} atoms bound with CaM. However, CaM needs to bind at least three Ca^{2+} to be active. Among the four species of Ca^{2+}-bound CaM, only Ca_3CaM and Ca_4CaM are effective in regulating AC and PDE activities (4, 15, 34). Additional details of Ca^{2+}-bound CaM dynamics are discussed in the APPENDIX.

The dynamic intracellular concentrations of cAMP are determined by the rates of cAMP synthesis and degradation and can be mathematically expressed as shown in *Eq. 1*:

$$\frac{d[cAMP]_i}{dt} = V_{AC} - V_{PDE} - k_d[cAMP]_i, \quad (1)$$

where V_{AC} is AC activity, V_{PDE} is PDE activity, and k_d is a coefficient of PDE-independent cAMP destruction, which we fit as $k_d = 0.01\ s^{-1}$.

Rodent β-cells and insulinoma cell lines express several AC isoforms, including the Ca^{2+}/CaM-activated isoforms AC1, AC3, and AC8 (6, 18, 28, 29). Ca^{2+}-dependent regulation of AC has not been specifically examined in the β-cell. To overcome this problem, we incorporated elements of a model describing Ca^{2+}-dependent regulation of AC in *Aplysia* neuron R15 (42). In this model, Ca^{2+}-activated AC is stimulated by Ca^{2+}/CaM at low $[Ca^{2+}]$ (<10 μM) and inhibited by free Ca^{2+} at extremely high $[Ca^{2+}]_i$ (>10 μM) (42).

In our model, Ca_3CaM and Ca_4CaM were considered equally efficient in regulating the Ca^{2+}-dependent AC and PDE activities, as was proposed by Yu et al. (42). This mechanism was simulated by the product of two first-order Michaelis-Menten-type kinetic equations, one fitting the stimulatory half of the bimodal curve and the other fitting the inhibitory half of the bimodal curve (42). AC activity is also dependent on the concentration of ATP ([ATP]). However, based on our previous analysis, we have assumed that [ATP] is close to constant (in the range of 3–6 mM) in the β-cell (11). Since [ATP] is much greater than the K_m for ACs, the equation for AC activity does not include the term [ATP]. In this case, the equation for AC can be combined with that of Ca^{2+}/CaM-independent AC isoform and can be written as

$$V_{AC} = V_{ACG} + V_{mCAM} \times \left[\frac{[Ca_3CaM]_i + [Ca_4CaM]_i}{[Ca_3CaM]_i + [Ca_4CaM]_i + K_{P,CaM}} \times \frac{K_{N,Ca}}{K_{N,Ca} + [Ca^{2+}]_i}\right], \quad (2)$$

where V_{ACG} is the activity of Ca^{2+}/CaM-independent AC, V_{mCAM} is the basal level of Ca^{2+}/CaM-dependent AC activity, $K_{N,Ca}$ is the half-maximal value of $[Ca^{2+}]_i$ for the inhibition of AC by free Ca^{2+} (75 μM; derived from Ref. 42), and $K_{P,CaM}$ is the half-maximal value of ($[Ca_3CaM] + [Ca_4CaM]$) for the stimulation of AC by Ca^{2+}/CaM.

We have focused on properties of the Ca^{2+}/CaM-dependent isoform AC8, since that seems to be predominant in β-cells (6). This isoform has very low activity in the absence of free Ca^{2+}. The half-maximal activating concentration for free Ca^{2+} is 0.5 μM (when CaM is added) (9), corresponding to $K_{P,CaM} = 0.348$ μM.

cAMP undergoes hydrolysis to the biologically inactive 5′-AMP by PDEs. PDE isoforms are characterized by differences in their substrate specificity (e.g., cAMP vs. cGMP), kinetics, allosteric regulation, and tissue distribution (13, 15). Both islets and β-cell lines contain PDE1, the Ca^{2+}/CaM-activated PDE (13). A member of the Ca^{2+}-activated PDE1 family, PDE1C, was found to be expressed in MIN6 cells along with several other PDE isoforms (28). A first-order kinetics equation was used to describe the relationship between Ca^{2+}-activated PDE and Ca^{2+}/CaM (27, 42). The general kinetics equation from Ref. 42, with an additional term for the Ca^{2+}/CaM-independent PDE form, can be written as

$$V_{PDE} = \left[V_{GPDE} + V_{CAPDE} \times \left(\beta_{PDE} + K_{mod,PDE}\frac{[Ca_3CaM]_i + [Ca_4CaM]_i}{[Ca_3CaM]_i + [Ca_4CaM]_i + K_{DPDE}}\right)\right] \times \frac{[cAMP]_i}{K_{PDE} + [cAMP]_i}, \quad (3)$$

where V_{GPDE} represents the activity of Ca^{2+}/CaM-independent PDE, V_{CAPDE} is the basal level of Ca^{2+}/CaM-dependent PDE activity, β_{PDE} is a constant (0.4; derived from Ref. 42), $K_{mod,PDE}$ is a scaling factor (1.2; derived from Ref. 42) that defines the dynamic range of PDE activity when activated by Ca^{2+}, and K_{DPDE} is the half-maximal value of ($[Ca_3CaM] + [Ca_4CaM]$). The half-maximal value for free Ca^{2+} (when CaM is added) varies from 0.27 to 3 μM for different isoforms of PDE (41). We suggest, similarly to the AC dependence, that K_{DPDE} is ~0.348 μM. This is consistent with the half-maximal value for that of free Ca^{2+}, which is equal to 0.5 μM (see above). The rate of this enzyme reaction is also determined by [cAMP]; the equation for PDE activity includes terms for $[cAMP]_i$, where K_{PDE} is the half-maximal value of $[cAMP]_i$ (3.0 μM; derived from Ref. 42).

The complete system consists of seven state variables employed in the previous model (11, 12) and two new variables, $[CaCaM]_i$ and $[cAMP]_i$. Nine differential equations describe their behavior, including *Eq. A1* (in APPENDIX) for $[CaCaM]_i$ and *Eq. 1* for $[cAMP]_i$. Simulations were performed using the software environment as described previously (11, 12).

RESULTS

Effect of Glucose and GLP-1 on cAMP Formation

We used Epac1-camps to determine the effect of secretagogues on $[cAMP]_i$. Stimulation with 20 mM glucose increases Ca^{2+} and cAMP concentration in MIN6 cells (28). $[Ca^{2+}]_i$ oscillations were generated by application of glucose (20 mM) and tetraethylammonium chloride (TEA), an inhibitor of K^+ channels (Fig. 2). In agreement with previous results (28), this treatment generated concomitant Ca^{2+} and cAMP oscillations that were typically out of phase. We also investigated $[cAMP]_i$ changes induced by GLP-1. GLP-1 induced slow Ca^{2+} oscillations measured in MIN6, and $[cAMP]_i$ oscillations were in phase with Ca^{2+} oscillations (Fig. 3).

Specific Features of the Model

Previously published experimental data for $[cAMP]_i$ dynamics were obtained under relative steady-state conditions or during slow Ca^{2+} oscillations with periods of several minutes. Data for $[cAMP]_i$ dynamics during fast Ca^{2+} oscillations in β-cells with periods ranging from 5 to 20 s are not yet

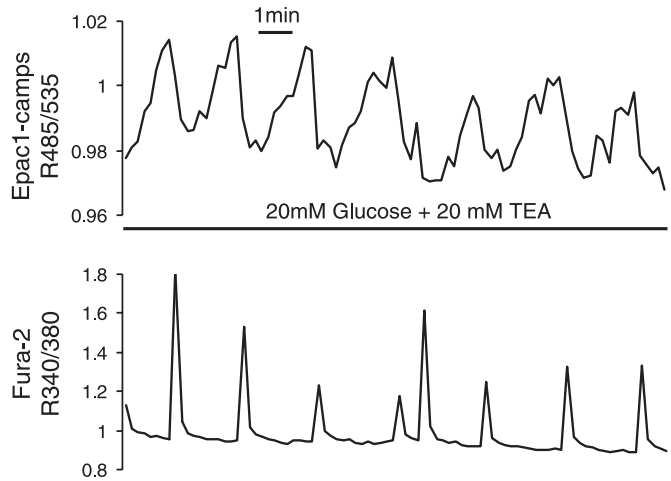

Fig. 2. Ca^{2+} and cAMP oscillations in glucose-stimulated MIN6 cells. Simultaneous imaging of cytosolic cAMP concentration ($[cAMP]_I$; *top* trace, $R_{485/535}$) and cytosolic Ca2+ concentration ($[Ca^{2+}]_I$; *bottom* trace, $R_{340/380}$) in a single MIN6 cell stimulated with 20 mM glucose and 20 mM tetraethylammonium chloride (TEA). Note that second messenger oscillations were out of phase, with each $[Ca^{2+}]_i$ spike coupled to a rapid and transient reduction in $[cAMP]_i$.

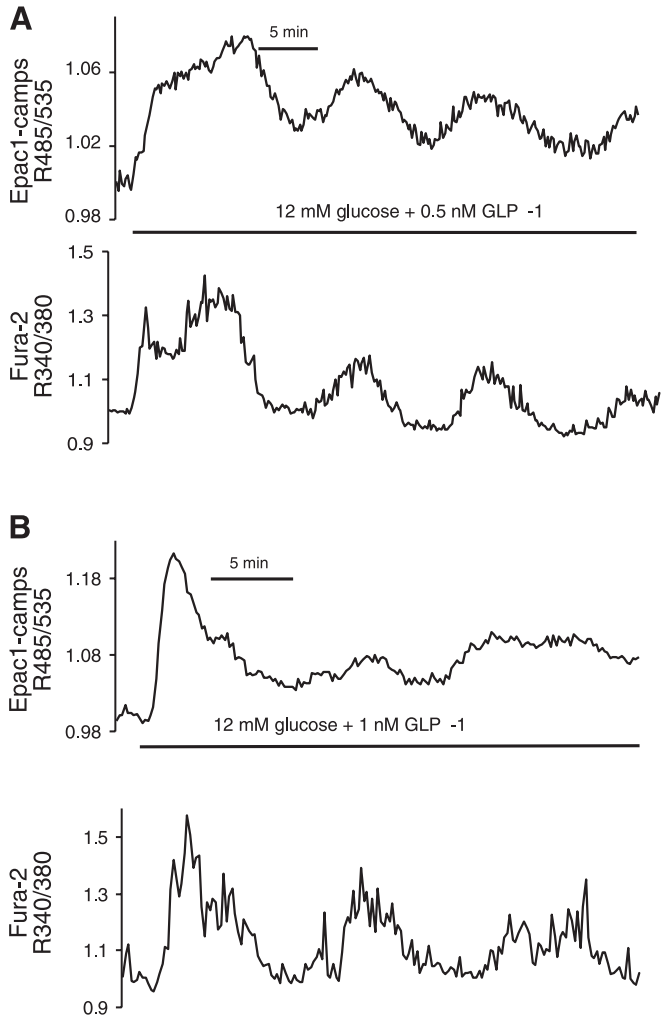

Fig. 3. Glucagon-like peptide 1 (GLP-1) stimulated intracellular Ca^{2+} and cAMP oscillations in individual MIN6 β-cells. *A* and *B*: simultaneous imaging of $[cAMP]_i$ (*top* trace, $R_{485/535}$) and $[Ca^{2+}]_i$ (*bottom* trace, $R_{340/380}$) in single fura-2-loaded cells transiently expressing Epac1-camps stimulated with 0.5 (*A*) and 1 nM GLP-1 (*B*). Note the phasic relationship of cAMP and Ca^{2+} oscillations in these cells.

available, and so the results of modeling cannot be readily validated under conditions of fast Ca^{2+} oscillations. We therefore focused our tests of the model on simulations of steady-state and slow $[Ca^{2+}]_i$ and $[cAMP]_i$ oscillations. A simulation of fast Ca^{2+} and $[cAMP]_i$ oscillations was used for frequency analysis and as a prediction of possible experimental results.

A delay occurs between changes in $[Ca^{2+}]_i$ and corresponding changes in $[cAMP]_i$ levels. This lag may reflect delayed responses of the signaling pathways activating AC or PDE (8, 28, 40). We have modeled this delay by setting the maximal activities of AC and PDE isoforms at levels that replicate experimental slow $[cAMP]_i$ dynamics.

It was pointed out in the Introduction that activation of the cAMP signaling system can result in changes of the conductances of different ion channels. Although the ways in which cAMP quantitatively acts on these channels are not well understood, we were able to simulate several effects of the cAMP signaling system on ion channels by altering specific channel conductances in our previously published general model of the β-cell (11, 12). For example, an increase in VDCC conductance leads initially to a generation of slow $[Ca^{2+}]_i$ oscillations and then to an enhancement of Ca^{2+} channel amplitude and frequency (Fig. 4*A*). Decreasing K_{ATP} channel conductance leads to generation of slow $[Ca^{2+}]_i$ oscillations or even to an abrogation of existing $[Ca^{2+}]_i$ oscillations while maintaining an increased $[Ca^{2+}]$ level (Fig. 4*B*).

Characteristics of the experimental effects of increased cAMP in the β-cell include the generation of slow $[Ca^{2+}]_i$ oscillations or the modification of existing $[Ca^{2+}]_i$ oscillations, including enhancement of their amplitude and frequency or even their abrogation, while maintaining an increased $[Ca^{2+}]$ (see Refs. 2, 35). All of these effects may be due to an indirect effect of $[cAMP]_i$ leading to increased and/or decreased conductances of different channels. Our simulations illustrate such possibilities, although we did not model the mechanisms of these potential interactions.

cAMP Dynamics

The maximum amplitude of $[Ca^{2+}]_i$ is usually well below 10 μM in pancreatic β-cells, the concentration at which free Ca^{2+} substantially inhibits AC. For this reason, although free $[Ca^{2+}]_i$ is included in the equation describing AC activity (*Eq. 2*), the results are focused primarily on the role of Ca^{2+}/CaM. We examined the ways in which the Ca^{2+} oscillations influence the behavior of Ca^{2+}/CaM while increasing activity of AC and PDE. In all cases, levels of different forms of Ca^{2+}/CaM also

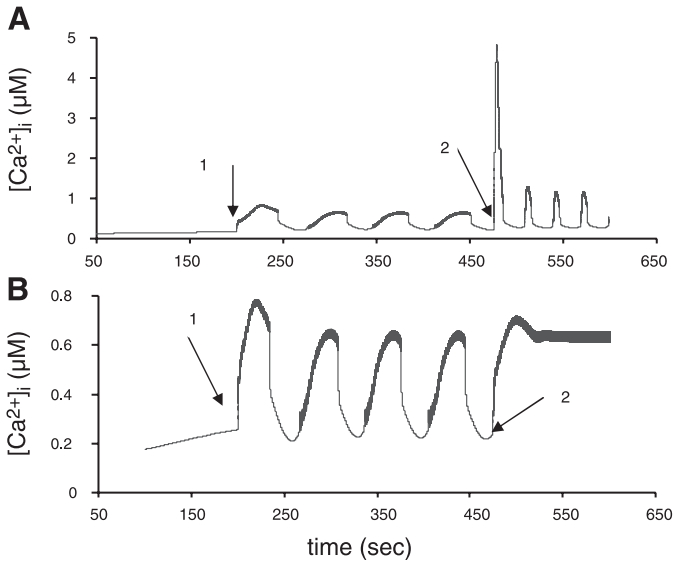

Fig. 4. Simulation of $[cAMP]_i$ effects on slow $[Ca^{2+}]_i$ oscillations. The simulation results from changes in the channel conductances at an intermediate glucose level (8 mM). *A*: influence on voltage-dependent Ca^{2+} channels (VDCCs). The initial maximum conductance for VDCCs was 400 pS. At this level the simulation does not show any $[Ca^{2+}]_i$ oscillations. At *arrow 1*, the maximum conductance for VDCCs was increased from 400 to 670 pS, which corresponds to base coefficients in our model (see Ref. 11), and $[Ca^{2+}]_i$ oscillations were initiated. At *arrow 2*, maximum conductance for VDCCs was increased from 670 to 1,300 pS and oscillations were amplified. *B*: influence on K_{ATP} channels. The initial maximum conductance for K_{ATP} channels was 50,000 pS, and $[Ca^{2+}]_i$ oscillations are absent. At *arrow 1*, the maximum conductance for K_{ATP} channels was decreased from 50,000 to 24,000 pS, leading to $[Ca^{2+}]_i$ oscillations. At *arrow 2*, maximum conductance for K_{ATP} channel was decreased from 24,000 to 5,000 pS, leading to the sustained, increased Ca^{2+} level.

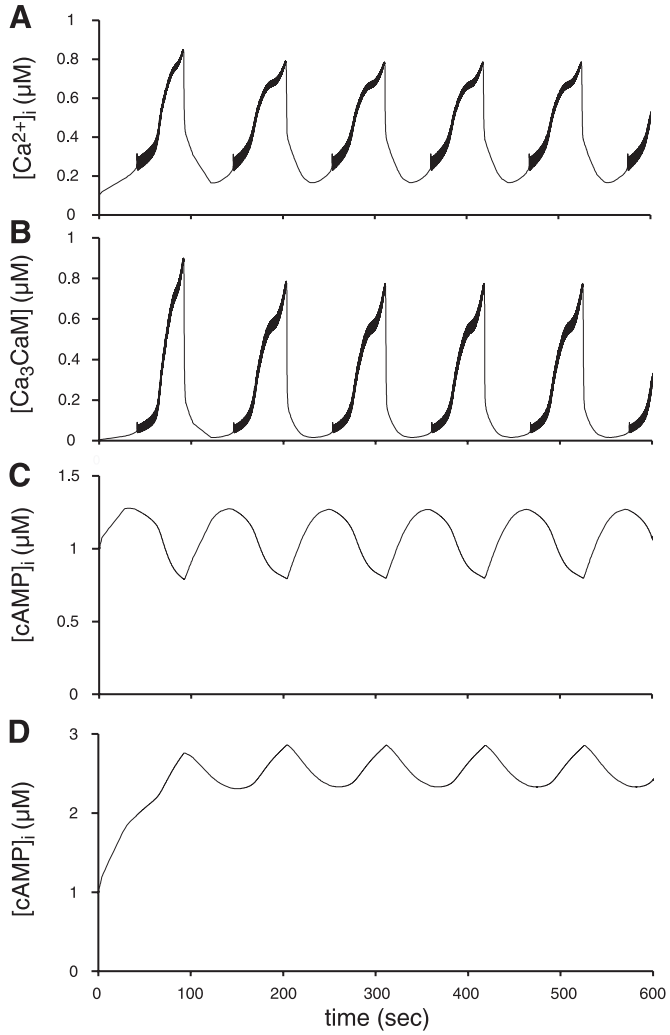

Fig. 5. A simulation of slow Ca^{2+} oscillations, $[Ca_3CaM]$, and $[cAMP]_i$ dynamics at an intermediate glucose level. *A*: the oscillations of $[Ca^{2+}]_i$ generated by the models are similar to those obtained previously (11), indicating that the extension to the model did not change the baseline activity. *B*: $[Ca_3CaM]$ oscillates in phase with free Ca^{2+}. Activities of Ca^{2+}/CaM-independent forms of AC and PDE are the same in every case (V_{ACG} = 0.00012 μmol/ms; V_{GPDE} = 0.00024 μmol/ms). The contribution of Ca^{2+}/CaM-dependent forms of AC and PDE to the regulation of $[cAMP]_i$ is different. *C*: Ca^{2+}/CaM-dependent PDE alone regulated by $[Ca^{2+}]_i$ (V_{mCaM} = 0; V_{CAPDE} = 0.00024 μmol/ms). $[cAMP]_i$ was approximately antiphasic to $[Ca^{2+}]_i$ oscillations. *D*: Ca^{2+}/CaM-dependent AC alone regulated by $[Ca^{2+}]_i$ (V_{mCaM} = 0.00005 μmol/ms; V_{CAPDE} = 0). $[cAMP]_i$ was in phase with $[Ca^{2+}]_i$. V_{ACG}, activity of Ca^{2+}/CaM-independent AC; V_{GPDE}, activity of Ca^{2+}/CaM-independent PDE; V_{mCAM}, basal level of Ca^{2+}/CaM-dependent AC activity; V_{CAPDE}, basal level of Ca^{2+}/CaM-dependent PDE activity.

oscillate in our model parallel to oscillations of free $[Ca^{2+}]_i$ and have the same phase (Fig. 5, *A* and *B*). This is because, according to *Eqs. A1–A5* (in APPENDIX), only changes of $[Ca^{2+}]_i$ can generate the alterations in concentrations of Ca^{2+}/CaM. However, because $[Ca_3CaM]$ is much greater than $[Ca_4CaM]$ (see Ref. 42), $[Ca_3CaM]_i$ plays the major role in regulating cAMP synthesis and degradation. $[Ca_3CaM]$ oscillates at a greater amplitude than $[Ca^{2+}]_i$ (Fig. 5) because all forms of Ca^{2+}/CaM are sensitive to $[Ca^{2+}]_i$ (*Eqs. A1–A4*, APPENDIX), and their cooperative binding leads to increased $[Ca^{2+}]_i$ sensitivity. Because Ca_3CaM and Ca_4CaM mediate the effect of Ca^{2+} on AC and PDE, this implies that Ca^{2+} effects are amplified at the level of CaM, as was reported in a model of Ca^{2+} and cAMP signaling dynamics in *Aplysia* neurons (42).

Dynamics of $[cAMP]_i$ depend on both the isoforms and activity of AC and PDE. An antiphasic relationship exists between $[Ca^{2+}]_i$ and $[cAMP]_i$ if we take into account only Ca^{2+}/CaM-dependent PDE and neglect Ca^{2+}/CaM-dependent AC (Fig. 5, *A* and *C*). If Ca^{2+}/CaM-dependent AC drives coupling between Ca^{2+} and cAMP in the absence of Ca^{2+}/CaM-dependent PDE, the calculated levels of cAMP are in phase with slow Ca^{2+} oscillations (Fig. 5, *A* and *D*). These effects can be explained by $[Ca^{2+}]_i$ activation of cAMP synthesis when Ca^{2+}/CaM-dependent AC is specifically activated or by increased cAMP degradation following activation of Ca^{2+}/CaM-dependent PDE (cf. Ref. 42).

With this computational background in place, we tested combinations of different isoforms of AC and PDE that might fit the published data on β-cell cAMP dynamics. The activities of AC and PDE were fit to suit the requirements for slow $[cAMP]_i$ transitions in response to $[Ca^{2+}]_i$ changes. The results of this combination with low activity of Ca^{2+}/CaM-dependent AC are shown in Fig. 6*A*, whereas Fig. 6*B* shows results obtained when the activity of Ca^{2+}/CaM-dependent AC was increased fivefold. Low Ca^{2+}/CaM-dependent AC activity leads to an antiphasic relationship between $[Ca^{2+}]_i$ and $[cAMP]_i$, because Ca^{2+}/CaM-dependent PDE is the predominant factor in these conditions (Fig. 6*A*). Increased Ca^{2+}/CaM-dependent AC activity leads to altered dynamics when the calculated level of cAMP is in phase with slow Ca^{2+} oscillations, because Ca^{2+}/CaM-dependent AC activity then dominates the regulation of cAMP synthesis (Fig. 6*B*).

We simulated the effects of low (Fig. 7) and high (Fig. 8) Ca^{2+}/CaM-dependent AC activity while changing $[Ca^{2+}]_i$. Application of VDCC inhibitors, to decrease $[Ca^{2+}]_i$, was simulated by decreasing the conductance for VDCCs (Figs. 7*A* and 8*A*). (Decreasing external $[Ca^{2+}]$ leads to the same result; not shown.) This causes a rapid decrease in $[Ca^{2+}]_i$ and cessation of the $[Ca^{2+}]_i$ and $[cAMP]_i$ oscillations, suggesting that dissipation of $[cAMP]_i$ oscillations is due to a termination of slow $[Ca^{2+}]_i$ oscillations. However, the precise behavior of

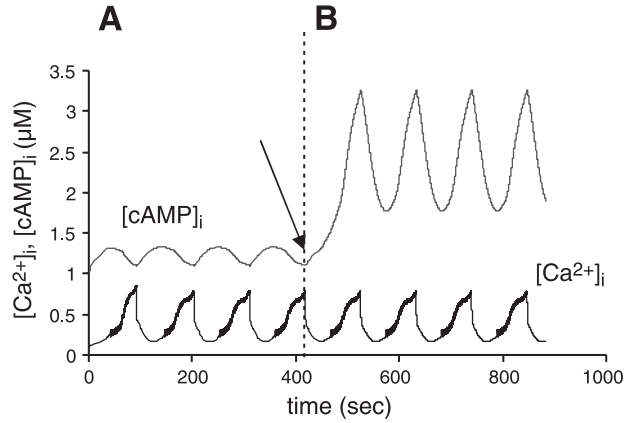

Fig. 6. Contribution of AC and PDE to cAMP dynamics when both AC and PDE are regulated by Ca^{2+}/CaM. *A*: Ca^{2+}/CaM-dependent PDE activity was higher than Ca^{2+}/CaM-dependent AC activity (V_{ACG} = 0.00024 μmol/ms; V_{mCaM} = 0.00005 μmol/ms; V_{GPDE} = 0.00024 μmol/ms; V_{CAPDE} = 0.00012 μmol/ms). *B*: Ca^{2+}/CaM-dependent AC activity (V_{mCaM}) was increased 5-fold (from 0.00005 to 0.0003 μmol/ms; arrow).

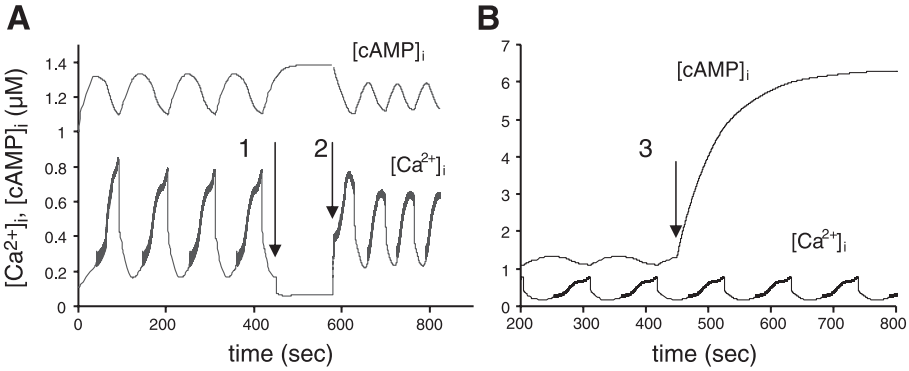

Fig. 7. Simulations under conditions of low Ca^{2+}/CaM-dependent AC activity. Coefficients were the same as in Fig. 6*A*. Application of a VDCC channel inhibitor was simulated by decreased VDCC conductance. *A*: at *arrow 1*, the maximum conductance for VDCCs was decreased from 670 to 100 pS, and at *arrow 2* it was restored. *B*: at *arrow 3*, the administration of a nonspecific PDE inhibitor was simulated by decreasing maximal activity of both phosphodiesterase forms 4-fold (V_{GPDE} and V_{CAPDE} were decreased from 0.00024 to 0.00006 μmol/ms).

cAMP concentration depends on several conditions. Unlike $[Ca^{2+}]_i$, $[cAMP]_i$ increases during low Ca^{2+}/CaM-dependent AC activity (Fig. 7*A*). With decreased synthesis, increased [cAMP] under these conditions is due to decreased degradation. Indeed, decreased Ca^{2+}/CaM-dependent PDE activity with decreased $[Ca^{2+}]_i$ by itself leads to increased $[cAMP]_i$. cAMP synthesis from Ca^{2+}/CaM-dependent AC under these conditions is already low, and any further decrease due to decreased $[Ca^{2+}]$ is insignificant. Otherwise, $[cAMP]_i$ decreases together with $[Ca^{2+}]_i$ when Ca^{2+}/CaM-dependent AC activity is increased (Fig. 8*A*). In this situation, cAMP biosynthesis as well as $[cAMP]_i$ are determined by high activity of Ca^{2+}/CaM-dependent AC and decrease with falling $[Ca^{2+}]_i$.

In the next simulation, administration of a nonspecific phosphodiesterase inhibitor was simulated by a fourfold decrease in maximal activity of PDEs (Figs. 7*B* and 8*B*). Decreased PDE activity should increase $[cAMP]_i$, and indeed it does in the model. However, $[cAMP]_i$ oscillations disappear (Fig. 7*B*). This effect is due to the inhibition of Ca^{2+}/CaM-dependent PDE, leading to equivalent activities of Ca^{2+}/CaM-dependent AC and PDEs. The rates of cAMP synthesis and degradation change uniformly with $[Ca^{2+}]_i$ oscillations, and $[cAMP]_i$ does not oscillate significantly. However, when AC activity predominates, the results are different. In the second case, $[cAMP]_i$ oscillations occur (Fig. 8*B*) because they are determined by increased Ca^{2+}/CaM-dependent AC activity, and inhibition of Ca^{2+}/CaM-dependent PDE does not change this effect.

We also modeled the response of $[cAMP]_i$ oscillations to changes in the $[Ca^{2+}]_i$ oscillation frequency (Fig. 9). Fast $[Ca^{2+}]_i$ oscillations were simulated by decreasing the specific coefficient k_{IP}, which is the rate constant for IP_3 production in our general model for $[Ca^{2+}]_i$ dynamics (for details, see Ref. 11). The period of fast $[Ca^{2+}]_i$ oscillations was changed from 60 to 10 s by decreasing the specific coefficient P_{leak}, which is the rate constant for a Ca^{2+} leak permeability from the ER in our general model for $[Ca^{2+}]_i$ oscillations (cf. Ref. 11). Although the amplitude of the simulated $[Ca^{2+}]_i$ oscillations was invariant, the amplitude of the $[cAMP]_i$ oscillations decreased drastically with increased frequency of $[Ca^{2+}]_i$ oscillations. This suggests that the cAMP system can act as a low-pass filter at higher frequencies of $[Ca^{2+}]_i$ oscillations. This effect can be explained by the inherent delays as a property of the cAMP biosynthesis system that we have simulated by setting the activities of AC and PDE to low levels.

Modeling the effect of increased Ca^{2+}-dependent AC activity at low $[Ca^{2+}]_i$ showed only modest effects on $[cAMP]_i$ (Fig. 10*A*). This result was obtained to simulate low glucose concentration in the medium when $[Ca^{2+}]_i$ is low. This is in contrast to the large increase in [cAMP] at high $[Ca^{2+}]_i$, as a simulation of increased glucose (Fig. 10*B*). This interesting effect can be explained as follows: at low glucose (and correspondingly low $[Ca^{2+}]_i$), activation of Ca^{2+}/CaM-dependent AC does not lead to a significant increase in rate of cAMP synthesis. This is because at low $[Ca^{2+}]_i$, cAMP synthesis is determined mainly by Ca^{2+}/CaM-independent AC activity. With increased glucose content (and correspondingly increased $[Ca^{2+}]_i$), the same increase in Ca^{2+}/CaM-dependent AC maximal activity does lead to an increase in cAMP synthesis (Fig. 10*B*), because increased $[Ca^{2+}]_i$ activates this isoform.

The dynamics of Ca^{2+}/CaM were represented by a single differential equation for $[CaCaM]_i$ to simplify the general model. Other Ca^{2+}/CaM forms were considered to be in equilibrium with $[CaCaM]_i$ (see APPENDIX). We also performed a simulation of the general model including three other forms of Ca^{2+}/CaM as the differential equations to test the effect of our simplification. We found that the amplitude of the $[cAMP]_i$

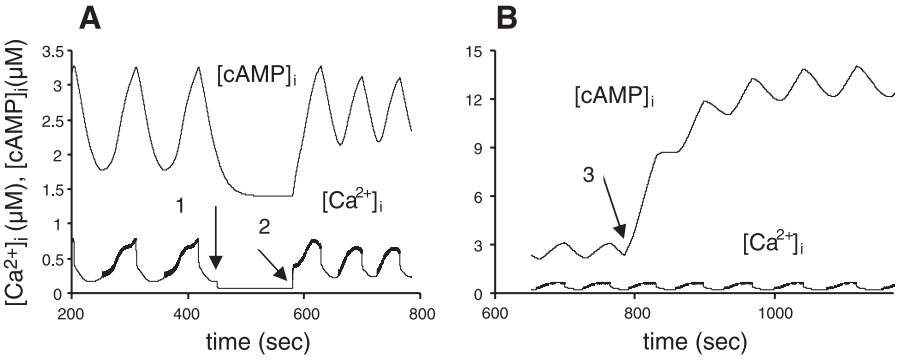

Fig. 8. Simulations during increased Ca^{2+}/CaM-dependent AC activity. Coefficients were the same as in Fig. 6*B*, where Ca^{2+}/CaM-dependent AC activity (V_{mCaM}) was increased 5-fold for comparison with the simulation in Fig. 7. Application of a VDCC inhibitor (at *arrow 1*; *A*) and a nonspecific PDE inhibitor (at *arrow 3*; *B*) was simulated as described in Fig. 7.

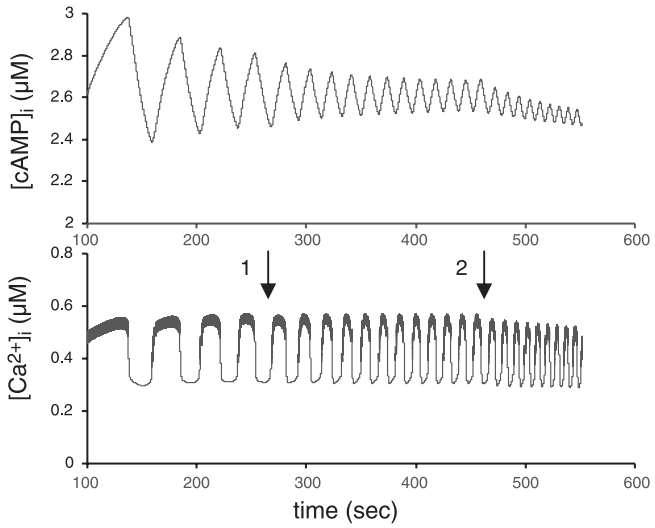

Fig. 9. Effect of the frequency of Ca^{2+} oscillations on the amplitude of cAMP oscillations. Fast $[Ca^{2+}]_i$ oscillations were simulated by decreasing the coefficient k_{IP}, the rate constant for IP_3 production, from 0.0003 to 0.0001 μmol/ms (see Ref. 11 for details of the simulation of fast $[Ca^{2+}]_i$ oscillations) at a glucose level of 10 mM. The change of $[Ca^{2+}]_i$ frequency was made using the coefficient P_{leak}, the rate constant for a Ca^{2+} leak permeability from the ER in our general model for $[Ca^{2+}]_i$ dynamics (see Ref. 11 for details). The initial value of this coefficient was 0.000115 pl/ms. At *arrow 1*, coefficient P_{leak} was decreased to 0.00011 pl/ms. At *arrow 2*, the coefficient was decreased to 0.000103 pl/ms.

was diminished only by up to 10% at high-frequency $[Ca^{2+}]_i$ oscillations (i.e., several per minute), similar to those in Fig. 9, *right*. Other simulations with slow $[Ca^{2+}]_i$ oscillations were virtually unchanged (not shown), and we suggest that our simplification can be correctly used in the simulations of steady-state and slow $[cAMP]_i$ dynamics.

DISCUSSION

We present an integrated model of β-cell cAMP dynamics with testable predictions and representative data. The model couples $[Ca^{2+}]_i$ regulation of specific Ca^{2+}-sensitive ACs and PDEs that give rise to synchronous or asynchronous oscillations or to monophasic changes in [cAMP]. Our previous model served as the basis for simulation of Ca^{2+} dynamics. However, any model of independent fast and slow Ca^{2+} oscillations (see, for example, Refs. 1, 3), when coupled with *Eqs. 1–3* and *A1–A5*, will lead to similar alterations in cAMP dynamics. Therefore, our ability to model cAMP dynamics is not a specific feature of the particular model of Ca^{2+} dynamics. The results from our model are a general characteristic of cAMP dynamics when $[Ca^{2+}]_i$ levels are a driving force for changes in $[cAMP]_i$.

Glucose/TEA-Induced cAMP Regulation

Using our model, we have evaluated several experimental results related to β-cell cAMP measurements. In one example, the combination of glucose stimulation plus TEA, an inhibitor of K^+ channels, induced depolarization-dependent $[Ca^{2+}]_i$ and $[cAMP]_i$ oscillations in insulin-secreting β-cell lines (Fig. 2 and Ref. 28). The mean frequency of the coupled Ca^{2+} and $[cAMP]_i$ oscillations was ~120 s (Fig. 2 and Fig. 5*A* from Ref. 28), which corresponds to slow $[Ca^{2+}]_i$ oscillations. However, oscillations of $[cAMP]_i$ were almost antiphasic to oscillations of $[Ca^{2+}]_i$. Landa et al. (28) found rapid cessation of the Ca^{2+} oscillations with decreased $[Ca^{2+}]_i$ when the β-cells were superfused with Ca^{2+}-free solutions (Fig. 5*C* from Ref. 28) or when a VDCC inhibitor (nitrendipine) was applied (Fig. 5*D* from Ref. 28). Under these conditions, [cAMP] oscillations were also ablated; however, unlike $[Ca^{2+}]_i$, $[cAMP]_i$ increased. Administration of the PDE inhibitor 3-isobutyl-1-methylxanthine (IBMX) abolished [cAMP] oscillations and increased $[cAMP]_i$ (Fig. 5*E* from Ref. 28). IBMX did not inhibit $[Ca^{2+}]_i$ oscillations. Increased $[cAMP]_i$ due to IBMX was also seen by Dyachok et al. (Ref. 8, their Fig. 3*a*) in INS-1 cells, where Ca^{2+} oscillations were enhanced as well.

These results were closely simulated in our model, assuming a relatively low activity of Ca^{2+}/CaM-dependent AC (Fig. 7). Our analysis shows that $[cAMP]_i$ dynamics in these experiments are due to low Ca^{2+}/CaM-dependent AC activity under these experimental conditions and that mainly Ca^{2+}-dependent PDE isoforms determine $[cAMP]_i$ dynamics. Therefore, this analysis supports the proposal by Landa et al. (28) that the dynamic effects of glucose on [cAMP] regulation are consistent with activation of a Ca^{2+}-dependent PDE isoform.

However, our simulation of glucose effects does not include the early transition data upon initial addition of glucose. Glucose stimulation alone has been reported to lead to either unchanged (8) or increased (6, 28, 39) steady-state $[cAMP]_i$. Simulated activation of Ca^{2+}-dependent PDE isoforms with both increased glucose and $[Ca^{2+}]_i$ in our model leads to decreased $[cAMP]_i$ (Fig. 10, *A* and *B*), but this result does not affect the dynamic part of the model. To explain the apparent contradiction, we note that there are several potential mechanisms for activation of specific AC isoforms following glucose stimulation that are not included in our model, including

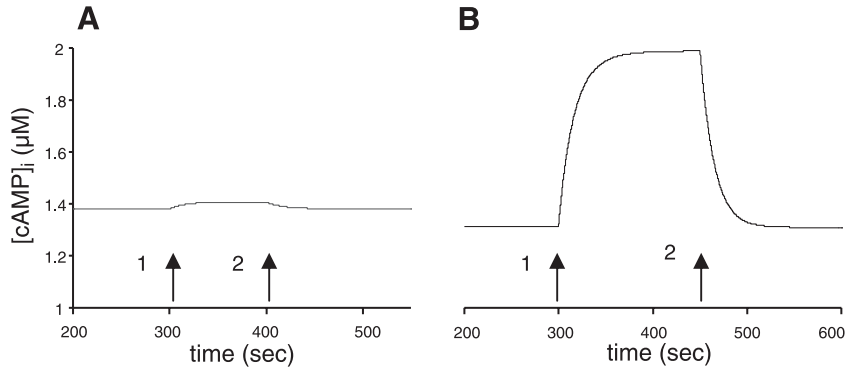

Fig. 10. Simulations of the effect of Ca^{2+}/CaM-dependent AC activation on increased cAMP levels at different glucose levels. *A*: low glucose level (4 mM) and initial low Ca^{2+}/CaM-dependent AC activity (initial coefficients were the same as in Fig. 6*A*). $[Ca^{2+}]$i was 0.084 μM. At *arrow 1*, maximum Ca^{2+}/CaM-dependent AC activity was increased from 0.00005 to 0.0003 μmol/ms (up to the same level as in Fig. 6*B*), and at *arrow 2* it was restored. *B*: simulation at high glucose level (10 mM). To avoid $[Ca^{2+}]_i$ oscillations, intracellular Na^+ level was frozen at its mean value (6.9 mM; see Ref. 12 for details of this method). In this case $[Ca^{2+}]_i$ was constant (0.29 μM). Other conditions were the same as in *A*.

membrane potential depolarization, activation of capacitative Ca^{2+} or cation entry, or activation by the phosphoinositide signaling pathway (reviewed in Ref. 4). All these processes can, potentially, lead to activation of AC and to increased $[cAMP]_i$. While intriguing, studies supporting these ideas are primarily qualitative, and there is a lack of adequate data for mathematical modeling. For this reason, we have not yet included these processes in our model.

The simulated slow changes in [cAMP] closely approximated the existing data. For example, according to Dyachok et al. (8), IBMX resulted in an increase in $[cAMP]_i$, with an average half-maximal time of 23 s. We simulated these data (Fig. 7), and the corresponding time was 35 s.

A similar result was obtained by modeling inhibition of AC. The GLP-1-induced $[cAMP]_i$ elevation was rapidly reversed following inhibition of AC by norepinephrine with a half-maximal suppression time of ~12 s (8). We simulated this decrease in $[cAMP]_i$ by reducing AC activity (Fig. 10*B*) and found that the corresponding half-time for decreased $[cAMP]_i$ was 10 s, again in close agreement with Dyachok et al. (8).

The effect of fast Ca^{2+} oscillations (3–4 oscillations per minute) in β-cells on cAMP dynamics is unknown. Our simulations (Fig. 9) as well as measurements of cAMP in human embryonic kidney cells (40) show that the amplitude of $[cAMP]_i$ oscillations decreases sharply when $[Ca^{2+}]_i$ oscillates at a frequency of 3–5 oscillations per minute. This suggests that $[cAMP]_i$ oscillations may be undetectable during fast $[Ca^{2+}]_i$ oscillations in β-cells.

Receptor-Induced cAMP Regulation

Insulin-secreting INS-1 cells responded to GLP-1 with pronounced slow $[Ca^{2+}]_i$ and $[cAMP]_i$ oscillations, which were in phase (8). MIN6 cells exhibited a similar response (Fig. 3). $[Ca^{2+}]_i$ and $[cAMP]_i$ oscillations induced by GLP-1 immediately disappeared following reduction of extracellular $[Ca^{2+}]$, causing a drop in $[Ca^{2+}]_i$. The $[cAMP]_i$ also decreased (Fig. 2*b* from Ref. 8). This effect was reversible with restoration of normal external $[Ca^{2+}]$, demonstrating the importance of dynamic regulation by Ca^{2+}. These results are similar to those obtained in our simulations with increased Ca^{2+}/CaM-dependent AC activity (Fig. 8). This means that, according to our model, the action of GLP-1 can be explained in part by an increase in the specific Ca^{2+}/CaM-dependent AC activity.

Increasing the glucose concentration from 3 to 20 mM markedly enhanced the response to GLP-1 but had a negligible effect on $[cAMP]_i$ (8), consistent with synergy between glucose and GLP-1 on cAMP production (6). This effect seems to be due to a small increase in $[cAMP]_i$ following GLP-1 stimulation at low glucose levels, simulated in Fig. 10*A*. This is consistent with low activity of Ca^{2+}/CaM-dependent AC when $[Ca^{2+}]_i$ is low (see RESULTS). Thus our model was able to simulate the empirical observations on the modest effect of GLP-1 under low-glucose conditions by the simple suggestion that GLP-1 specifically increased Ca^{2+}/CaM-dependent AC activity, rather than Ca^{2+}-independent AC isoforms. This mechanism describing the initial GLP-1 effect was proposed by Delmeire et al. (6), who found abundant expression of the Ca^{2+}/CaM-dependent type AC8 isoform in β-cells. Our analysis of the dynamic properties of cAMP regulation supports a pivotal role of Ca^{2+}-dependent AC activation in the action of GLP-1 receptor agonists.

GLP-1 Receptor Agonists and Specific Targets in Insulin Secretion

One noted advantage of GLP-1 agonists in the treatment of diabetes is that they increase insulin secretion only at stimulatory glucose concentrations, contributing to a low risk of hypoglycemia (22). This can be explained by the amplifying effect of increased glucose level on glucagon (or GLP-1)-induced cAMP production (6, 8). According to our simulation (Fig. 10), this effect stems from the increased activity of Ca^{2+}/CaM-dependent AC isoforms by increased $[Ca^{2+}]_i$.

On the other hand, sulfonylureas (e.g., tolbutamide) induce insulin secretion by directly inhibiting K_{ATP} channels, leading to increased $[Ca^{2+}]_i$ even in the presence of low extracellular glucose levels (30). However, according to our simulation (Fig. 10*B*), increased $[Ca^{2+}]_i$ should be sufficient for activation of Ca^{2+}/CaM-dependent AC and, consequently, for activation by GLP-1 receptor agonists even at low extracellular glucose concentrations.

Indeed, GLP-1 and tolbutamide applied simultaneously in 3 mM glucose increased insulin secretion significantly in the in situ perfused rat pancreas so that the effect of GLP-1 was uncoupled from its usual glucose dependence (5). Since the incidence of hypoglycemia increases if GLP-1 (or its analogs) are used together with sulfonylureas, the clinical combination of K_{ATP} blockers and GLP-1 agonists requires caution (36). This confirms the ability of our model to evaluate the effect of GLP-1 agonists on insulin secretion.

Role of cAMP Oscillations in Pancreatic β-Cells

We suggest that $[Ca^{2+}]_i$ oscillations function as a pacemaker for $[cAMP]_i$ oscillations in pancreatic β-cells. This follows from our dynamic simulations of $[cAMP]_i$ based on independent $[Ca^{2+}]_i$ oscillations, leading to simulation of different types of $[cAMP]_i$ oscillations similar to experimental results. This suggestion is also supported by data showing that a PDE inhibitor (IBMX) abolished $[cAMP]_i$ oscillations while not inhibiting $[Ca^{2+}]_i$ oscillations (Fig. 5*E* in Ref. 28) and by the finding that IBMX can stimulate $[Ca^{2+}]_i$ oscillations even during elevated, nonoscillating cAMP levels (8). Willoughby and Cooper (40) also suggested that $[Ca^{2+}]_i$ oscillations can be a pacemaker for cAMP oscillations in human embryonic kidney cells (HEK-293) transfected with the Ca^{2+}-sensitive cyclase isoform AC8. They found that "artificial" cytosolic Ca^{2+} oscillations with frequencies lower than 3 min^{-1} induced cAMP oscillations (40). These oscillations were "in phase" with $[Ca^{2+}]_i$ changes. This corresponds to our simulations employing AC8 as the main Ca^{2+}-dependent isoform (Fig. 5*B* in Ref. 8). However, it is also possible that in other cell types, cAMP oscillations could be a product of interactions among cAMP, Ca^{2+}, and agents that stimulate cAMP synthesis or decrease its breakdown (see, for example, Refs. 16, 31).

Oscillations of $[cAMP]_i$ levels may have significant biological implications, even though they are not a pacemaker for $[Ca^{2+}]_i$ oscillations. Oscillating $[cAMP]_i$ may exert substantially different effects on downstream targets than would a constant level of $[cAMP]_i$. For example, pulsatile changes in $[cAMP]_i$ are more efficient in inducing the release of certain

hormones (19, 38). Since an increase in $[cAMP]_i$ activates insulin secretion in β-cells, it is possible that oscillating $[cAMP]_i$ in phase with $[Ca^{2+}]_i$ in response to GLP-1 treatment would facilitate this process. Other potential effects such as regulating gene expression require further study.

Effect of cAMP on Ion Channels

Agents that increase cAMP in the β-cell typically stimulate or modify $[Ca^{2+}]_i$ oscillations. This includes enhancement of amplitude and frequency or even abrogation of existing $[Ca^{2+}]_i$ oscillations while maintaining an increased $[Ca^{2+}]$ level (2, 10, 35). We were able to simulate these effects (Fig. 4) by taking into account the different mechanisms proposed for downstream cAMP effects on specific β-cell channels. We simulated this by increasing activity of L-type Ca^{2+} channels (Fig. 4*A*) or reducing K_{ATP} channel conductance (Fig. 4*B*). The simulations were performed only as an illustration, since our model may not include the exact mechanisms by which cAMP modulates ion channels. The effects on Ca^{2+} dynamics are likely due to multiple actions of $[cAMP]_i$ on several pathways, not modeled in this study.

In conclusion, we have described an integrated model of pancreatic β-cell Ca^{2+} and cAMP dynamics. The model includes detailed descriptions of interactions among $[Ca^{2+}]_i$, Ca^{2+}/CaM, and cAMP regulation. It predicts that oscillations of cAMP levels may result from cytoplasmic Ca^{2+} oscillations, replicating published data. The phase shift between Ca^{2+} and cAMP oscillations is likely due to responses of specific isoforms of AC and PDE to $[Ca^{2+}]_i$, supported by the experimental results. This analysis of the dynamic data provides evidence for a pivotal role of Ca^{2+}-dependent AC activation in the action of GLP-1 agonists. The regulatory properties of AC and PDE isoforms contribute to the characteristic dynamics of cAMP and explain a synergistic action of glucose and GLP-1 receptor agonists on insulin secretion.

APPENDIX

The dynamics of Ca^{2+} binding to CaM have been described previously in several models (33, 34, 42). We used as a basis for Ca^{2+}/CaM modeling the recent model by Yu et al. (42), where the rate constants were obtained from studies with cultured mammalian cells. However, in our model, Ca_2CaM, Ca_3CaM, and Ca_4CaM can be considered to be in equilibrium with CaCaM, because we have taken into account primarily steady-state and slow processes (on the order of minutes) in β-cells, and this has been a reasonable simplification (see RESULTS). We ignored the role of CaM changes in the total Ca^{2+} buffer, because CaM is only 10% of the total Ca^{2+} buffer (42). After these simplifications, the model for Ca^{2+}/CaM regulation (derived from Ref. 42) can be written as

$$\frac{d[CaCaM]_i}{dt} = k_{1f}[Ca]_i[CaM]_i - k_{1b}[CaCaM]_i, \quad (A1)$$

$$[Ca_2CaM]_i = (k_{2f}/k_{2b})[Ca]_i[CaCaM]_i \quad (A2)$$

$$[Ca_3CaM]_i = (k_{3f}/k_{3b})[Ca]_i[Ca_2CaM]_i \quad (A3)$$

$$[Ca_4CaM]_i = (k_{4f}/k_{4b})[Ca]_i[Ca_3CaM]_i \quad (A4)$$

$$[CaM]_i = CaM_o - [CaCaM]_i - [Ca_2CaM]_i - [Ca_3CaM]_i - [Ca_4CaM]_i, \quad (A5)$$

where k_{1f}–k_{4f} are the forward rate constants and k_{1b}–k_{4b} are the backward rate constants in the four steps of Ca^{2+} binding to CaM. Each Ca in the equations refers to Ca^{2+}. The rate constants are as follows: $k_{1f} = 2.3\ \mu M^{-1}\cdot ms^{-1}$, $k_{2f} = 2.3\ \mu M^{-1}\cdot ms^{-1}$, $k_{3f} = 160\ \mu M^{-1}\cdot ms^{-1}$, $k_{4f} = 160\ \mu M^{-1}\cdot ms^{-1}$, $k_{1b} = 2.4\ ms^{-1}$, $k_{2b} = 2.4\ ms^{-1}$, $k_{3b} = 405\ ms^{-1}$, and $k_{4b} = 405\ ms^{-1}$ (cf. Ref. 42). In all simulations the total concentration of CaM ($[CaM]_i$) was 11.25 μM (42).

ACKNOWLEDGMENTS

We thank Drs. J. Sturis and N. Tamarina for fruitful discussions.

GRANTS

This work was partially supported by National Institute of Diabetes and Digestive and Kidney Diseases Grants DK20595 and DK48494.

REFERENCES

1. **Bertram R, Satin L, Zhang M, Smolen P, Sherman A.** Calcium and glycolysis mediate multiple bursting modes in pancreatic islets. *Biophys J* 87: 3074–3087, 2004.
2. **Bode HP, Moormann B, Dabew R, Goke B.** Glucagon-like peptide 1 elevates cytosolic calcium in pancreatic beta-cells independently of protein kinase A. *Endocrinology* 140: 3919–3927, 1999.
3. **Chay TR.** Effects of extracellular calcium on electrical bursting and intracellular and luminal calcium oscillations in insulin secreting pancreatic β-cells. *Biophys J* 73: 1673–1688, 1997.
4. **Cooper DMF.** Regulation and organization of adenylyl cyclases and cAMP. *Biochem J* 375: 517–529, 2003.
5. **De Heer J, Holst JJ.** Sulfonylurea compounds uncouple the glucose dependence of the insulinotropic effect of glucagon-like peptide 1. *Diabetes* 56: 438–443, 2006.
6. **Delmeire D, Flamez D, Hinke SA, Cali JJ, Pipeleers D, Schuit F.** Type VIII adenylyl cyclase in rat beta cells: coincidence signal detector/generator for glucose and GLP-1. *Diabetologia* 46: 1383–1393, 2003.
7. **Dyachok O, Gylfe E.** Ca^{2+}-induced Ca^{2+} release via inositol 1,4,5-trisphosphate receptors is amplified by protein kinase A and triggers exocytosis in pancreatic β-cells. *J Biol Chem* 279: 45455–45461, 2004.
8. **Dyachok O, Isakov Y, Sagetorp J, Tengholm A.** Oscillations of cyclic AMP in hormone-stimulated insulin-secreting β-cells. *Nature* 439: 349–352, 2006.
9. **Fagan KA, Mahey R, Cooper DM.** Functional co-localization of transfected Ca^{2+}-stimulable adenylyl cyclases with capacitative Ca^{2+} entry sites. *J Biol Chem* 271: 12438–12444, 1996.
10. **Flamez D, Gilon P, Moens K, Van Breusegem A, Delmeire D, Scrocchi LA, Henquin JC, Drucker DJ, Schuit F.** Altered cAMP and Ca^{2+} signaling in mouse pancreatic islets with glucagon-like peptide-1 receptor null phenotype. *Diabetes* 48: 1979–1986, 1999.
11. **Fridlyand LE, Ma L, Philipson LH.** Adenine nucleotide regulation in pancreatic β-cells: modeling of ATP/ADP-Ca^{2+} interactions. *Am J Physiol Endocrinol Metab* 289: E839–E848, 2005.
12. **Fridlyand LE, Tamarina N, Philipson LH.** Modeling of Ca^{2+} flux in pancreatic β-cells: role of the plasma membrane and intracellular stores. *Am J Physiol Endocrinol Metab* 285: E138–E154, 2003.
13. **Furman B, Pyne N, Flatt P, O'Harte F.** Targeting beta-cell cyclic 3′5′ adenosine monophosphate for the development of novel drugs for treating type 2 diabetes mellitus. A review. *J Pharm Pharmacol* 56: 1477–1492, 2004.
14. **Goraya TA, Cooper DM.** Ca^{2+}-calmodulin-dependent phosphodiesterase (PDE1): current perspectives. *Cell Signal* 17: 789–797, 2005.
15. **Goraya TA, Masada N, Ciruela A, Cooper DM.** Sustained entry of Ca^{2+} is required to activate Ca^{2+}-calmodulin-dependent phosphodiesterase 1A. *J Biol Chem* 279: 40494–40504, 2004.
16. **Gorbunova YV, Spitzer NC.** Dynamic interactions of cyclic AMP transients and spontaneous Ca^{2+} spikes. *Nature* 418: 93–96, 2002.
17. **Gromada J, BrockB, Schmitz O, Rorsman P.** Glucagon-like peptide-1: regulation of insulin secretion and therapeutic potential. *Basic Clin Pharmacol Toxicol* 95: 252–262, 2004.
18. **Guenifi A, Portela-Gomes GM, Grimelius L, Efendic S, Abdel-Halim SM.** Adenylyl cyclase isoform expression in non-diabetic and diabetic Goto-Kakizaki (GK) rat pancreas. Evidence for distinct overexpression of type-8 adenylyl cyclase in diabetic GK rat islets. *Histochem Cell Biol* 113: 81–89, 2000.
19. **Haisenleder DJ, Yasin M, Marshall JC.** Enhanced effectiveness of pulsatile 3′,5′-cyclic adenosine monophosphate in stimulating prolactin and alpha-subunit gene expression. *Endocrinology* 131: 3027–3033, 1992.

20. **Harbeck MC, Chepurny O, Nikolaev VO, Lohse MJ, Holz GG, Roe MW.** Simultaneous optical measurements of cytosolic Ca^{2+} and cAMP in single cells. *Sci STKE* 2006: pl6, 2006.
21. **Harndahl L, Jing XJ, Ivarsson R, Degerman E, Ahren B, Manganiello VC, Renstrom E, Holst LS.** Important role of phosphodiesterase 3B for the stimulatory action of cAMP on pancreatic beta-cell exocytosis and release of insulin. *J Biol Chem* 277: 37446–37455, 2002.
22. **Holz GG.** New insights concerning the glucose-dependent insulin secretagogue action of glucagon-like peptide-1 in pancreatic beta-cells. *Horm Metab Res* 36: 787–794, 2004.
23. **Holz GG, Leech CA, Heller RS, Castonguay M, Habener JF.** cAMP-dependent mobilization of intracellular Ca^{2+} stores by activation of ryanodine receptors in pancreatic beta-cells. A Ca^{2+} signaling system stimulated by the insulinotropic hormone glucagon-like peptide-1-(7-37). *J Biol Chem* 274: 14147–14156, 1999.
24. **Kang G, Chepurny OG, Malester B, Rindler MJ, Rehmann H, Bos JL, Schwede F, Coetzee WA, Holz GG.** cAMP sensor Epac as a determinant of ATP-sensitive potassium channel activity in human pancreatic beta cells and rat INS-1 cells. *J Physiol* 573: 595–609, 2006.
25. **Kang G, Chepurny OG, Rindler MJ, Collis L, Chepurny Z, Li WH, Harbeck M, Roe MW, Holz GG.** A cAMP and Ca^{2+} coincidence detector in support of Ca^{2+}-induced Ca^{2+} release in mouse pancreatic beta cells. *J Physiol* 566: 173–188, 2005.
26. **Kanno T, Suga S, Wu J, Kimura M, Wakui M.** Intracellular cAMP potentiates voltage-dependent activation of L-type Ca^{2+} channels in rat islet beta-cells. *Pflügers Arch* 435: 578–580, 1998.
27. **Kramer RH, Levitan ES, Wilson MP, Levitan IB.** Mechanism of calcium-dependent inactivation of a potassium current in *Aplysia* neuron R15: interaction between calcium and cyclic AMP. *J Neurosci* 8: 1804–1813, 1988.
28. **Landa LR Jr, Harbeck M, Kaihara K, Chepurny O, Kitiphongspattana K, Graf O, Nikolaev VO, Lohse MJ, Holz GG, Roe MW.** Interplay of Ca^{2+} and cAMP signaling in the insulin-secreting MIN6 beta-cell line. *J Biol Chem* 280: 31294–32302, 2005.
29. **Leech CA, Castonguay MA, Habener JF.** Expression of adenylyl cyclase subtypes in pancreatic beta-cells. *Biochem Biophys Res Commun* 27: 703–706, 1999.
30. **MacDonald PE, Joseph JW, Rorsman P.** Glucose-sensing mechanisms in pancreatic beta-cells. *Philos Trans R Soc Lond B Biol Sci* 360: 2211–2225, 2005.
31. **Maeda M, Lu S, Shaulsky G, Miyazaki Y, Kuwayama H, Tanaka Y, Kuspa A, Loomis WF.** Periodic signaling controlled by an oscillatory circuit that includes protein kinases ERK2 and PKA. *Science* 304: 875–878, 2004.
32. **Nikolaev VO, Bunemann M, Hein L, Hannawacker A, Lohse MJ.** Novel single chain cAMP sensors for receptor-induced signal propagation. *J Biol Chem* 279: 37215–37218, 2004.
33. **Persechini A, Cronk B.** The relationship between the free concentrations of Ca^{2+} and Ca^{2+}-calmodulin in intact cells. *J Biol Chem* 274: 6827–6830, 1999.
34. **Rasmussen H, Barrett PQ.** Calcium messenger system: an integrated view. *Physiol Rev* 64: 938–984, 1984.
35. **Sasaki S, Nakagaki I, Kondo H, Hori S.** Involvement of the ryanodine-sensitive Ca^{2+} store in GLP-1-induced Ca^{2+} oscillations in insulin-secreting HIT cells. *Pflügers Arch* 445: 342–351, 2002.
36. **Scot VJ.** Incretin mimetics as emerging treatments for type 2 diabetes. *Ann Pharmacother* 39: 110–118, 2005.
37. **Seino S, Shibasaki T.** PKA-dependent and PKA-independent pathways for cAMP-regulated exocytosis. *Physiol Rev* 85: 1303–1342, 2005.
38. **Vitalis EA, Costantin JL, Tsai PS, Sakakibara H, Paruthiyil S, Iiri T, Martini JF, Taga M, Choi AL, Charles AC, Weiner RI.** Role of the cAMP signaling pathway in the regulation of gonadotropin-releasing hormone secretion in GT1 cells. *Proc Natl Acad Sci USA* 97: 1861–1866, 2000.
39. **Wang JL, Corbett JA, Marshall CA, McDaniel ML.** Glucose-induced insulin secretion from purified beta-cells. A role for modulation of Ca^{2+} influx by cAMP- and protein kinase C-dependent signal transduction pathways. *J Biol Chem* 268: 7785–7791, 1993.
40. **Willoughby D, Cooper DMF.** Ca^{2+} stimulation of adenylyl cyclase generates dynamic oscillations in cyclic AMP. *J Cell Sci* 119: 828–836, 2006.
41. **Yan C, Zhao AZ, Bentley JK, Beavo JA.** The calmodulin-dependent phosphodiesterase gene PDE1C encodes several functionally different splice variants in a tissue-specific manner. *J Biol Chem* 271: 25699–25706, 1996.
42. **Yu X, Byrne JH, Baxter DA.** Modeling interactions between electrical activity and second-messenger cascades in *Aplysia* neuron R15. *J Neurophysiol* 91: 2297–2311, 2004.